

# Quantum and classical probability distributions for position and momentum

R. W. Robinett

*Department of Physics, The Pennsylvania State University, University Park, Pennsylvania 16802*

(Received 15 August 1994; accepted 16 November 1994)

The classical and quantum probability distributions for both position and momentum are compared for several model systems admitting bound states including the harmonic oscillator, the infinite well, and the linear confining potential ( $V(x) = F|x|$ ). Examples corresponding to unbound systems, including the uniformly accelerating particle and the motion of a particle moving away from a point of unstable equilibrium, i.e., the “unstable oscillator” defined by  $V(x) = -kx^2/2$ , are also considered. The quantum and classical distribution of kinetic and potential energy for the harmonic oscillator is briefly discussed. © 1995 American Association of Physics Teachers.

## I. INTRODUCTION

Textbooks and pedagogical articles on quantum mechanics present a variety of ways of making the connection between the Schrödinger wave function and the classical motion of particles. For free particles, for example, Gaussian wave packets constructed from plane wave solutions<sup>1</sup> are frequently presented as an analytic example. For bound states, wave packet solutions for the harmonic oscillator problem can be constructed<sup>2</sup> which explicitly exhibit the classical periodicity of the particle motion; when generalized to coherent states,<sup>3,4</sup> such wave packets can even make contact with so-called “squeezed states” and modern research. Numerical solutions of the Schrödinger equation representing wave packet scattering events have been extensively studied for one-<sup>5-10</sup> and two-dimensional<sup>11</sup> systems and help visualize the time dependence of such interactions.

Another familiar approach for stationary state solutions is to compare the probability density, given by  $P_{QM}(x;n) = |\psi_n(x)|^2$ , with a “classical probability distribution” and show that the two approach each other, in a locally averaged sense, in the correspondence principle limit of large quantum number  $n$ . This is often done using the harmonic oscillator as an example,<sup>12</sup> and this will be the starting point of our discussion as well.

Before proceeding, let us briefly contrast these two approaches and discuss the meaning of a classical probability distribution.<sup>12</sup> For a classical particle for which both the initial position and velocity are specified, the probability density for position can be written as  $P_{CL}(x) = \delta[x - x(t)]$  corresponding to a well-defined trajectory; this is the limit which wave packet solutions attempt to emulate. The quantum probability distribution given by  $|\psi(x;n)|^2$  corresponds most closely to a classical phase space distribution where only the energy,  $E = E_n$ , is precisely specified; such a classical distribution would be proportional to  $\delta[H(p,x) - E]$  where  $H(p,x)$  is the classical Hamiltonian. If no information on the momentum variable is required (or known), the distribution can be integrated over  $p$  yielding a classical probability density for the position coordinate. While one should not forget the fundamental differences between quantum and classical probability distributions (phase space distributions have no counterpart in standard quantum theory, for example), it is still instructive to examine their relationship in the correspondence principle limit.

Many texts also stress the importance of the momentum-space solution of the Schrödinger equation, either given by a Fourier transform of  $\psi(x)$ ,

$$\phi(p) = \frac{1}{\sqrt{2\pi\hbar}} \int_{-\infty}^{+\infty} dx \psi(x) e^{-ipx/\hbar}, \quad (1)$$

or else obtained directly as a solution of the Schrödinger equation in momentum space. The fact that  $\psi(x)$  and  $\phi(p)$  have the same information content, encoded in different but equivalent ways, and thus constitute two, complementary representations of the same quantum state is often discussed. The conceptual importance of the corresponding momentum-space probability distributions,  $P_{QM}(p) = |\phi(p)|^2$ , is of increasing relevance as related quantities are directly measurable in many fields of experimental physics research; examples include momentum distributions obtained from neutron scattering in solids and liquids, nuclear momentum distributions in nuclear scattering experiments, and parton (i.e., quark and gluon) distributions in the proton necessary for understanding the high energy collisions in elementary particle physics.

There are, however, relatively few instances where the comparison of quantum momentum probability densities<sup>13</sup> with their classical counterparts is made in the literature and we will present several such examples as the main content of this paper. Such examples can provide experience in visualizing the physical significance of  $|\phi(p)|^2$ , i.e., “thinking in  $p$ -space,” as well as reinforcing the connection between the quantum wave function, in this case  $\phi(p)$ , and the classical motion of particles. Since the notion of a classical probability distribution for the momentum variable is less familiar, it can also be useful to recall that the same classical phase-space distribution corresponding to constant energy mentioned above can be used to obtain  $P_{CL}(p)$  by integrating over the unmeasured  $x$  variable.

We begin in Sec. II by reviewing the notions of classical probability distributions for position for bound states using the harmonic oscillator as a familiar example and extend such ideas to visualize the sharing of kinetic and potential energy in the eigenstates of this system. We then define the notion of a classical probability distribution for momentum and compare it to the quantum equivalent,  $|\phi_n(p)|^2$ , especially in the large  $n$  limit. In Sec. III, we apply these notions to an even more familiar system, namely the infinite well potential, and then, in Sec. IV, turn to a discussion of the symmetric, confining linear potential, defined by  $V(x) = F|x|$ . For comparison, we then show how these ideas can also be applied to quantum wave functions describing particles which are unbound, even though the corresponding stationary state energy eigenfunctions are not normalizable. We present examples of the probability distributions for both

position and momentum for a particle moving away from a point of *unstable* equilibrium, described by an “unstable oscillator,” namely one with a potential of the form  $V(x) = -kx^2/2$  (Sec. V) as well as those for a uniformly accelerating particle, given by  $V(x) = Fx$  (Sec. VI).

## II. THE HARMONIC OSCILLATOR

Let us first review the notion of a classical probability distribution for position for a particle in a bound state in some one-dimensional potential well. The motion in such a situation is periodic, the particle bouncing back and forth between the classical turning points  $a$  and  $b$ ; the time for one traversal of the well (from, say, left to right) is half the period,  $\tau/2$ . The amount of time,  $dt$ , the particle spends in the small region of space,  $dx$ , near the point  $x$  is given by the speed there,  $v(x)$ , via

$$dt = \frac{dx}{v(x)} = \frac{dx}{v(x)}. \quad (2)$$

The probability of finding the particle in this small region is simply the ratio of this time to the total time for one traversal, that is

$$P_{CL}(x)dx \equiv \text{Probability}[(x, x+dx)] = \frac{dt}{\tau/2} = \frac{2}{\tau} \frac{dx}{v(x)} \quad (3)$$

so that

$$P_{CL}(x) = \frac{2}{\tau} \frac{1}{v(x)}, \quad (4)$$

which defines the classical probability density for position measurements. This definition shows that the particle will spend more time (and hence be measured more often) in regions where the classical speed is low. It also shows that the probability density is properly normalized since

$$\int_a^b P_{CL}(x)dx = \int_{t_a}^{t_b} \frac{dt}{\tau/2} = \frac{2}{\tau} (t_b - t_a) = 1. \quad (5)$$

Since the classical speed is related to the kinetic energy by  $T(x) = mv^2(x)/2$  and hence to the potential energy, we can write

$$P_{CL}(x) = \frac{2}{\tau} \sqrt{\frac{m}{2T(x)}} = \frac{2}{\tau} \sqrt{\frac{m}{2[E - V(x)]}}. \quad (6)$$

Thus the classical probability density is large (small) where the kinetic energy is small (large) or the potential energy is large (small). (We note that such ideas can also be motivated by using the WKB approximation.)

For the case of the simple harmonic oscillator we have  $V(x) = kx^2/2$ ,  $\tau = 2\pi\sqrt{k/m}$ , and the amplitude  $A$  is determined from the total energy via  $E = kA^2/2$ . In this case we find

$$P_{CL}(x) = \frac{1}{\pi} \frac{1}{\sqrt{A^2 - x^2}} \quad (7)$$

with the classical turning points at  $(-A, A)$  and one can easily check that Eq. (5) is satisfied.

The energy eigenfunctions and eigenvalues of the corresponding Schrödinger equation

$$-\frac{\hbar^2}{2m} \frac{d^2\psi(x)}{dx^2} + \frac{1}{2} kx^2 \psi(x) = E \psi(x) \quad (8)$$

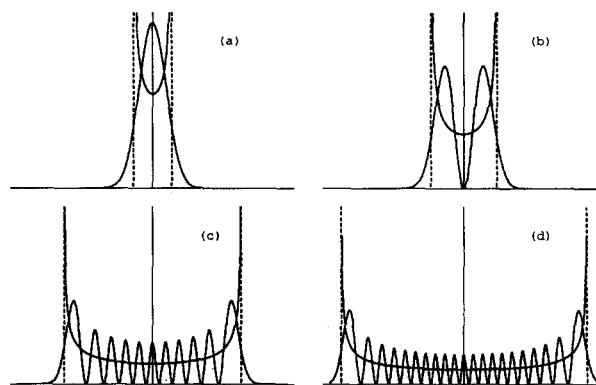


Fig. 1. The classical  $[P_{CL}(x)]$  and quantum  $[P_{QM}(x; n) = |\psi_n(x)|^2]$  position probability densities for the harmonic oscillator vs  $x$  for values of the quantum number  $n$  given by (a)  $n=0$ , (b)  $n=1$ , (c)  $n=10$ , and (d)  $n=20$ . The dotted lines correspond to the classical turning points.

are well known. The quantized energies are given by

$$E_n = (n + 1/2)\hbar\omega \quad n = 0, 1, 2, \dots, \quad (9)$$

where  $\omega = \sqrt{k/m}$  while the stationary states can be written in the form

$$\psi_n(x) = C_n h_n(y) e^{-y^2/2} \quad \text{where } y = \sqrt{\frac{m\omega}{\hbar}} x. \quad (10)$$

The  $h_n(y)$  are the Hermite polynomials of degree  $n$  and the normalization constants are

$$C_n = \left( \frac{\sqrt{m\omega/\hbar} \pi}{2^n n!} \right)^{1/2}. \quad (11)$$

The quantum probability density,  $P_{QM}(x; n) \equiv |\psi_n(x)|^2$ , is plotted along with its classical counterpart,  $P_{CL}(x)$  from Eq. (7), in Fig. 1 for values of  $n$  equal to 0, 1, 10, 20. For the classical distribution, the turning points are, of course, determined by the condition that  $E_n = (n + 1/2)\hbar\omega = E = kA^2/2$ . The equivalent of Fig. 1 is presented in many textbooks to illustrate that the quantum wave function, if averaged locally over a finite interval, does indeed seem to approach the classical distribution for  $n \rightarrow \infty$ ; a more formal statement of this might be that

$$\lim_{n \rightarrow \infty} \int_{x_1}^{x_2} |\psi_n(x)|^2 dx = \int_{x_1}^{x_2} P_{CL}(x) dx. \quad (12)$$

There is another nice way to visualize the connection between the classical trajectory and the probability distribution (which, after all, results from an “averaging” over the trajectory) which we illustrate in Fig. 2 for the case of the harmonic oscillator. Equal sized “bins” of width  $dx$  are selected on the vertical axis of the  $x(t)$  vs  $t$  plot and then projected horizontally until they intersect the trajectory curve. They are then projected down onto the  $t$  axis and the resulting time spent in the bin,  $dt$  is calculated and shown (plotted “sideways”) as a histogram on the vertical scale; infinitesimally small bin sizes will then reproduce the continuous distribution. (For periodic motion, this procedure need only be performed over a single period but this method is of some usefulness in the analysis of classical chaotic mo-

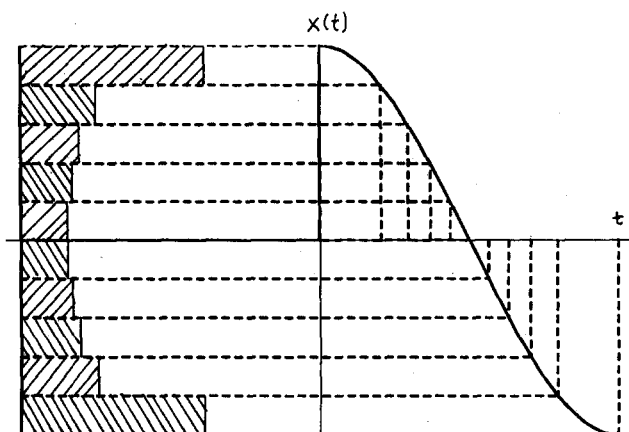


Fig. 2. The projection technique as applied to the trajectory plot  $[x(t) \text{ vs } t]$  corresponding to the sinusoidal motion of a particle undergoing simple harmonic motion.

tions when one has to average over much longer time scales.) This method is, of course, equivalent to the definition of Eq. (3), but shows it in a useful way.

Figure 1 also illustrates that the quantum wave function is “wigglier” (more nodes per unit increment of  $x$ ) in the middle than near the classical turning points which is consistent with energy sharing arguments; when the classical “spring” is unstretched near  $x \approx 0$ , the energy is mostly in the form of kinetic while near the turning points where the particle comes to rest and rebounds, the speed and hence kinetic energy go to zero and all the energy is stored as potential. This notion of the “wiggleness” of the  $\psi(x)$  being related to the local kinetic energy can be illustrated using a familiar relation. Many textbooks show that the expectation value of the kinetic energy operator can be written in the form

$$\begin{aligned} \langle \hat{T} \rangle &= \frac{1}{2m} \langle \hat{p}^2 \rangle = -\frac{\hbar^2}{2m} \int_{-\infty}^{+\infty} dx \psi^*(x) \frac{d^2 \psi(x)}{dx^2} \\ &\stackrel{\text{IBP}}{=} -\frac{\hbar^2}{2m} \left( \psi^*(x) \frac{d\psi(x)}{dx} \right)_{-\infty}^{+\infty} \\ &\quad + \frac{\hbar^2}{2m} \int_{-\infty}^{+\infty} dx \frac{d\psi^*(x)}{dx} \frac{d\psi(x)}{dx} \\ &= +\frac{\hbar^2}{2m} \int_{-\infty}^{+\infty} \left| \frac{d\psi(x)}{dx} \right|^2 dx, \end{aligned} \quad (13)$$

where IBP stands for an integration by parts and we drop the “surface” term by assuming that  $\psi(x)$  is sufficiently well behaved at  $x = \pm\infty$ . While not of great physical importance for comparing with real measurements, we can define for visualization purposes a quantum distribution for kinetic energy via

$$\tau_{\text{QM}}(x) \equiv \frac{\hbar^2}{2m} \left| \frac{d\psi(x)}{dx} \right|^2 \quad \text{where} \quad \langle \hat{T} \rangle = \int_{-\infty}^{+\infty} \tau(x) dx. \quad (14)$$

The corresponding quantity for potential energy might then be

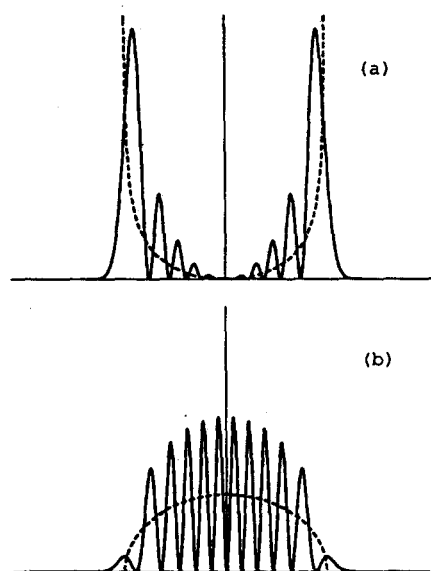


Fig. 3. The classical (dotted curve) and quantum (solid curve) for the distributions of potential energy (a) and kinetic energy (b) for the harmonic oscillator.

$$\nu_{\text{QM}}(x) \equiv V(x) |\psi(x)|^2 \quad \text{since} \quad \langle V \rangle = \int_{-\infty}^{+\infty} \nu(x) dx. \quad (15)$$

To make connection with the classical values, we can define

$$\tau_{\text{CL}}(x) \equiv P_{\text{CL}}(x) T(x) = P_{\text{CL}}(x) \frac{1}{2} m v^2(x) = P_{\text{CL}}(x) [E - V(x)] \quad (16)$$

and

$$\nu_{\text{CL}}(x) \equiv P_{\text{CL}}(x) V(x). \quad (17)$$

For the harmonic oscillator problem, we then have

$$\tau_{\text{CL}}(x) = \frac{k}{2\pi} \sqrt{A^2 - x^2} \quad \text{and} \quad \nu_{\text{CL}}(x) = \frac{k}{2\pi} \frac{x^2}{\sqrt{A^2 - x^2}}. \quad (18)$$

The integrals of these quantities give the average kinetic and potential energies and we find

$$\langle \tau_{\text{CL}} \rangle = \int_{-A}^{+A} \tau(x) dx = \frac{kA^2}{4}, \quad (19)$$

$$\langle \nu_{\text{CL}} \rangle = \int_{-A}^{+A} \nu(x) dx = \frac{kA^2}{4}, \quad (20)$$

i.e.,  $\langle V \rangle = \langle T \rangle$ , so that the energy is, on average, shared equally. This is a familiar result in both classical and quantum mechanics, which can be shown using the virial theorem or by direct calculation.

Perhaps more interestingly, we can compare the quantum [Eqs. (14) and (15)] and classical [Eqs. (16) and (17)] distributions of potential and kinetic energy in Fig. 3 (where  $n=10$  is used for the quantum case); Figure 3 helps to illustrate where the various forms of energy are “stored” in the harmonic oscillator and once again exhibits a correspondence principle connection.

These results have all been derived in the position-space representation of the quantum state and we wish to generalize these results to the momentum-space probability densi-

ties, both quantum and classical. The special symmetry inherent in the harmonic oscillator problem, in which  $x$  and  $p$  play similar roles, guarantees that the Schrödinger equation in momentum space for this problem has essentially the same form as Eq. (8), namely,

$$\frac{p^2}{2m} \phi(p) - \frac{\hbar^2 m \omega^2}{2} \frac{d^2 \phi(p)}{dp^2} = E \phi(p), \quad (21)$$

where one makes the association

$$\hat{p} = \frac{\hbar}{i} \frac{\partial}{\partial x} \Leftrightarrow p, \quad (22)$$

$$x \Leftrightarrow \hat{x} = i\hbar \frac{\partial}{\partial p}. \quad (23)$$

The solutions are easily obtained and one finds

$$\phi_n(p) = D_n h_n(q) e^{-q^2/2} \quad \text{where } q = \frac{p}{\sqrt{m\omega\hbar}} \quad (24)$$

with normalization constants

$$D_n = \left( \frac{1}{n! 2^n \sqrt{m\omega\hbar\pi}} \right)^{1/2}. \quad (25)$$

The momentum-space probability densities,  $P_{QM}(p; n) = |\phi_n(p)|^2$ , plotted as a function of the scaled variable  $q$ , therefore have exactly the same form as in Fig. 1.

To derive the corresponding classical momentum distribution, we begin, as before, by considering the probability of measuring the particle with momentum  $p$  to be

$$P_{CL}(p) dp \equiv \text{Probability}[(p, p+dp)] \\ = \frac{dt}{\tau/2} = \frac{2}{\tau} \frac{dp}{|dp/dt|}. \quad (26)$$

We then identify  $dp/dt$  with the classical force,

$$\frac{dp}{dt} = F(x) = -\frac{dV(x)}{dx} \quad (27)$$

so that

$$P_{CL}(p) = \frac{2}{\tau} \frac{1}{|F(x)|}. \quad (28)$$

[Note the "mixed" notation which implies that  $F(x)$  must somehow be written in terms of  $p$ .] For the case of the simple harmonic oscillator we have  $F(x) = -kx$  and  $V(x) = kx^2/2$  so

$$|F(x)| = \sqrt{2kV(x)} = \sqrt{2k(E - mv^2/2)} \\ = \sqrt{2k(E - p^2/2m)} = \sqrt{\frac{k}{m}(p_0^2 - p^2)}, \quad (29)$$

where  $E \equiv p_0^2/2m$  defines the maximum momentum. Using Eq. (28), this then gives

$$P_{CL}(p) = \frac{1}{\pi \sqrt{p_0^2 - p^2}} \quad (30)$$

since  $\tau = 2\pi\sqrt{k/m}$ . Thus the classical momentum distribution does have exactly the same form (as a function of  $p$ ) as the classical distribution of position, Eq. (7); this is consistent with the complete symmetry between  $x$  and  $p$  for the simple harmonic oscillator.

We can also generalize the projection of trajectory technique to visualize  $P_{CL}(p)$ . For the classical position space distribution, one projected the amount of time spent in equal  $x$  bins onto the vertical axis from a graph of  $x(t)$  vs  $t$  and the resulting binned values approached  $P_{CL}(x)$ . A knowledge of the exact trajectory,  $x(t)$ , implies that we can also plot  $v(t)$ , or equivalently and more usefully,  $p(t) = v(t)/m$  vs  $t$  and perform the same projection trick to obtain  $P_{CL}(p)$ . For the harmonic oscillator, since

$$x(t) = A \cos(\omega t + \phi) \quad \text{and} \quad p(t) = -\frac{A\omega}{m} \sin(\omega t + \phi) \quad (31)$$

both have the identical sinusoidal time dependence. Therefore, time bins projected onto the  $x$  and  $p$  axes are guaranteed to yield the same distribution in either case.

These observations are perhaps useful as a possible misconception about the classical momentum distribution can arise if one argues (incorrectly) along the following lines: "If we measure the position of the particle and find it most often near the classical turning points, then, since its momentum there is small, we expect that the  $P_{CL}(p)$  will be largest for  $|p| \approx 0$ ." This guess is, of course, exactly the opposite of what actually happens in the correspondence principle limit.

One can also generalize the quantum [Eqs. (14) and (15)] and classical distributions [Eqs. (16) and (17)] of kinetic and potential energy using momentum space variables and wave functions and we leave this as an exercise for the interested reader.

### III. THE INFINITE WELL

The infinite well problem provides another testing ground for these ideas as we now illustrate. We take, for definiteness, a symmetric well potential defined via

$$V(x) = \begin{cases} 0 & \text{for } |x| < a \\ +\infty & \text{for } |x| > a \end{cases} \quad (32)$$

For purposes of example, we will only consider the even solutions, namely

$$u_n^{(+)} = \frac{1}{\sqrt{a}} \cos\left(\frac{(n-1/2)\pi x}{a}\right), \quad n = 1, 2, 3, \dots \quad (33)$$

with energy eigenvalues

$$E_n^{(+)} = \frac{\hbar^2 (2n-1)^2 \pi^2}{8ma^2}. \quad (34)$$

The corresponding momentum space wave functions are easily found to be

$$\phi_n^{(+)}(p) = \frac{1}{\sqrt{2\pi\hbar}} \int_{-a}^{+a} dx u_n^{(+)}(x) e^{-ipx/\hbar} \\ = \sqrt{\frac{a}{2\pi\hbar}} \left( \frac{\sin[(n-1/2)\pi - ap/\hbar]}{[(n-1/2)\pi - ap/\hbar]} \right. \\ \left. + \frac{\sin[(n-1/2)\pi + ap/\hbar]}{[(n-1/2)\pi + ap/\hbar]} \right). \quad (35)$$

We plot both the position-space and momentum-space probability distributions,  $|u_n^{(+)}(x)|^2$  and  $|\phi_n^{(+)}(p)|^2$ , in Fig. 4 for  $n = 1, 3$ , and  $10$  and note that two well-defined peaks at  $p = \pm(n-1/2)\hbar/a$  are observed except for the ground state.

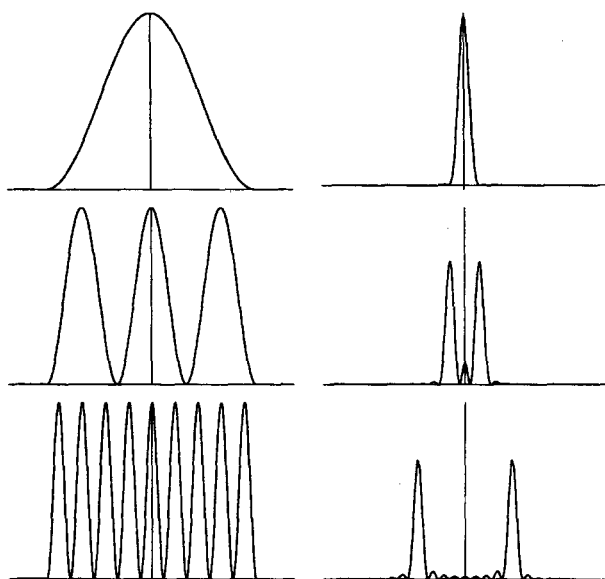


Fig. 4. The position-space (left-hand column) and momentum-space (right-hand column) probability densities for the symmetric infinite well corresponding to  $n=0, 1, 10$  (top, middle, bottom, respectively).

To make contact with the classical trajectories in the well, we plot  $x(t)$  and  $v(t)$  vs  $t$  in Fig. 5 and note that the constant speed motion in the well (the velocity changes sign after a bounce on the walls) implies that the classical distribution of probability will be a constant, specifically

$$P_{CL}(x) = \frac{2}{\tau} \sqrt{\frac{2m}{E}} = \frac{1}{2a} \quad (36)$$

since  $\tau = 4a/v$  and  $E = mv^2/2$ . This flat distribution of probability can also be seen via the projection technique using the  $x(t)$  vs  $t$  curve in Fig. 5. For large values of  $n$ , the  $\cos^2[(n-1/2)\pi x/a]$  term averages to  $1/2$  showing that the

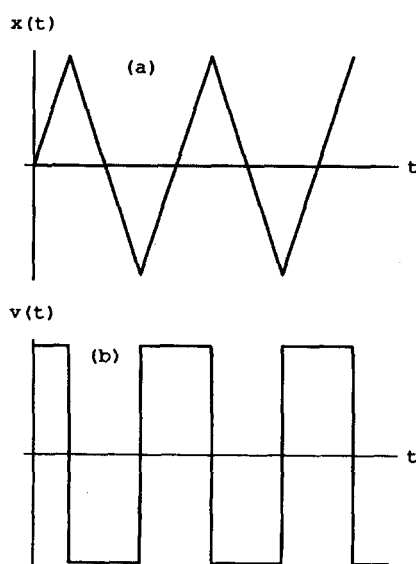


Fig. 5. The classical position  $x(t)$ , (a), and velocity  $v(t)$ , (b), for a particle in an infinite well potential.

quantum probability approaches the classical limit in this sense. The local averaging can actually be done analytically in this case giving

$$\begin{aligned} \text{Prob}[b < x < b+c] &= \int_b^{b+c} (u_n^{(+)}(x))^2 dx \\ &= \frac{c}{2a} + \frac{1}{(2n-1)\pi} \\ &\quad \times \left[ \sin\left(\frac{(2n-1)\pi(b+c)}{a}\right) - \sin\left(\frac{(2n-1)\pi b}{a}\right) \right] \\ &\rightarrow \frac{c}{2a} \text{ as } n \rightarrow \infty. \end{aligned} \quad (37)$$

The classical momentum distribution is more difficult to derive analytically but the projection technique applied to Fig. 5(b) clearly implies that only the two values  $P = \pm p_0 = \pm \sqrt{2mE}$  will be allowed. To see how this limit arises naturally from the quantum wave functions, we write the momentum space wave function in the form

$$\begin{aligned} \phi(p) &= \sqrt{\frac{\Delta p}{2\pi}} \left( \frac{\sin[(p_0-p)/\Delta p]}{(p_0-p)} \right) \\ &\quad + \frac{\sin[(p_0+p)/\Delta p]}{(p_0+p)}, \end{aligned} \quad (38)$$

where  $p_0 = (n-1/2)\pi\hbar/a = \sqrt{2mE_n^{(+)}}$  and  $\Delta p \equiv \hbar/a$ . We can take the corresponding momentum probability distribution,  $|\phi(p)|^2$ , in the limit that  $\Delta p \rightarrow 0$  (i.e., a macroscopic limit) and use a standard representation for the Dirac  $\delta$  function:

$$\lim_{\epsilon \rightarrow 0} \delta_\epsilon(x) = \lim_{\epsilon \rightarrow 0} \left[ \frac{\epsilon}{\pi} \frac{\sin^2(x/\epsilon)}{x^2} \right] = \delta(x). \quad (39)$$

Because the cross terms in  $|\phi(p)|^2$  vanish in the limit  $\hbar/a \rightarrow 0$ , we find that

$$\lim_{\hbar/a \rightarrow 0} |\phi(p)|^2 = \frac{1}{2} [\delta(p-p_0) + \delta(p+p_0)] = P_{CL}(p). \quad (40)$$

This is just a mathematical representation of the more intuitive statement made above.

#### IV. THE LINEAR POTENTIAL

While it is not as fundamentally important as the harmonic oscillator potential, the symmetric linear potential, defined via  $V(x) = F|x|$ , (where  $F > 0$ ) is treated at this level in several texts<sup>14,15</sup> and has several instructive features.

(1) The symmetry of the potential ensures that the solutions can be classified according to their parity and the application of boundary conditions giving the quantized energy levels in the case relies heavily on this fact.

(2) The modified linear potential given by

$$\tilde{V}(z) = \begin{cases} \infty & \text{for } z < 0, \\ mgz & \text{for } z > 0, \end{cases} \quad (41)$$

is the quantum equivalent of a "bouncing ball," i.e., a uniform gravitational field above a rigid flat surface. The solutions to the problem are just the odd states of the "full" linear potential.

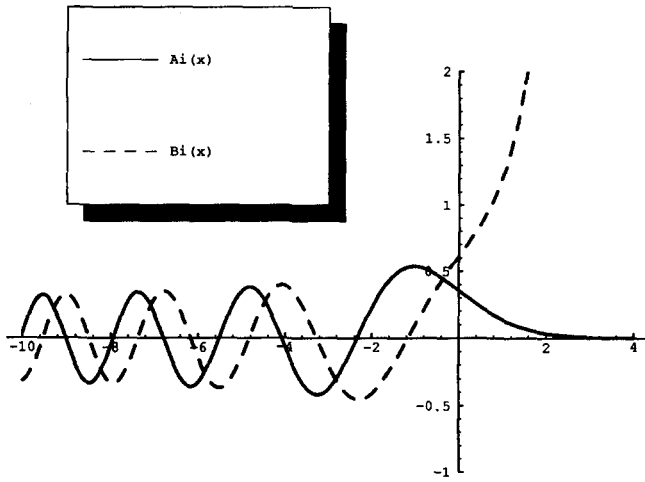


Fig. 6. Plot of the solutions to the Airy differential equation,  $Ai(x)$  and  $Bi(x)$ , vs  $x$ .

(3) It is argued that the theory governing the interactions of quarks and antiquarks (called quantum chromodynamics or QCD) in elementary particle physics implies that the non-relativistic limit of their interaction potential can be written as

$$V(r) = -\frac{4}{3} \frac{\alpha_s}{r} + Kr \quad (42)$$

so that at large separations the quark–antiquark pair feels a linear potential.

(4) Finally, it allows us a further check on the classical position and momentum distributions discussed above. We will also use many of the same mathematical results in discussing the uniformly accelerating particle in Sec. VI.

Using the symmetry of the potential we can argue that it is sufficient to solve the Schrödinger equation for  $x > 0$  only, i.e.,

$$-\frac{\hbar^2}{2m} \frac{d^2 \psi(x)}{dx^2} + Fx \psi(x) = E \psi(x) \quad (43)$$

for even  $[\psi^{(+)}(x)]$  and odd  $[\psi^{(-)}(x)]$  states and extend them to negatives values of  $x$  by using

$$\psi^{(+)}(-x) = \psi^{(+)}(x) \quad \text{and} \quad \psi^{(-)}(-x) = -\psi^{(-)}(x). \quad (44)$$

To accomplish this, we change variables to  $x = \rho y + \sigma$  (with  $\rho$  and  $\sigma$  to be determined) to simplify Eq. (43) and find the result

$$\frac{d^2 \psi(y)}{dy^2} = y \psi(y) \quad (45)$$

provided we define

$$\rho = \left( \frac{\hbar^2}{2mF} \right)^{1/3} \quad \text{and} \quad \sigma = \frac{E}{F}. \quad (46)$$

This is the Airy differential equation which has two, linearly independent solutions  $Ai(y)$ ,  $Bi(y)$  which are shown in Fig. 6; we will discuss the physical significance of these solutions at greater length in Sec. VI. The behavior of  $Bi(y)$  for large

$y$  is unacceptable (it diverges), so we have the (unnormalized) solution

$$\psi(x) = N Ai \left( \frac{x - \sigma}{\rho} \right) \quad \text{for } x > 0 \quad (47)$$

which is extended to  $x < 0$  via Eq. (44).

In this case, the boundary conditions at infinity have been easily implemented (much like the case of the *finite* square well) so the quantized energy eigenvalues are determined by matching the solutions at the boundary between two regions where the solutions are defined differently, namely at the origin. Because of the symmetry we must have

even solutions:

$$\psi^{(+)}(0) = \text{arbitrary} \quad \frac{d\psi^{(+)}(0)}{dx} = Ai' \left( -\frac{\sigma}{\rho} \right) = 0, \quad (48)$$

odd solutions:

$$\frac{d\psi^{(-)}(0)}{dx} = \text{arbitrary} \quad \psi^{(-)}(0) = Ai \left( -\frac{\sigma}{\rho} \right) = 0. \quad (49)$$

If we label the zeroes of the  $Ai'(y)$  and  $Ai(y)$  functions  $-y_i^{(+)}$  and  $-y_i^{(-)}$ , respectively, these conditions determine the quantized energy eigenvalues since

$$E_i^{(\pm)} = y_i^{(\pm)} \left( \frac{\hbar^2 F^2}{2m} \right)^{1/3}. \quad (50)$$

The first few zeros are given by

$$\begin{aligned} y_1^{(+)} &= 1.0188, & y_1^{(-)} &= 2.3381, \\ y_2^{(+)} &= 3.2482, & y_2^{(-)} &= 4.0879, \\ y_3^{(+)} &= 4.8201, & y_3^{(-)} &= 5.5206, \\ y_4^{(+)} &= 6.1633, & y_4^{(-)} &= 6.7867. \end{aligned} \quad (51)$$

(The energies are not evenly spaced and one can show that for large quantum number  $n$  the energies go as  $E_n \propto n^{2/3}$ , consistent with WKB quantization arguments.)

After normalizing the wave functions suitably [i.e., determining  $N$  in Eq. (47), which must be done numerically], one can obtain the position-space wave functions,  $|\psi_n^{(\pm)}(x)|^2$  and these can be compared to the classical probability distribution in the large  $n$  limit; we show this in Fig. 7 for two even wave functions corresponding to  $n=0, 14$ ; the results are quite similar to Fig. 1 for the harmonic oscillator. More interestingly, the momentum space wave functions and the corresponding  $P_{QM}(p)$  can be obtained through a numerical Fourier transform and are shown in Fig. 8. These (heavily numerical) calculations are relatively easily done using modern multipurpose computer mathematics packages such as Mathematica.<sup>16</sup>

The classical motion is easy enough to derive as the constant acceleration implies linearly increasing (or decreasing) velocities as in Fig. 9(b) with the position coordinate increasing (or decreasing) quadratically in time [Fig. 9(a)]. The classical position and momentum probabilities can then be derived using Eqs. (6) and (28) with the results

$$P_{CL}(x) = \frac{1}{4\sqrt{A}} \frac{1}{\sqrt{A-|x|}} \quad \text{for } |x| < A \quad (52)$$

and

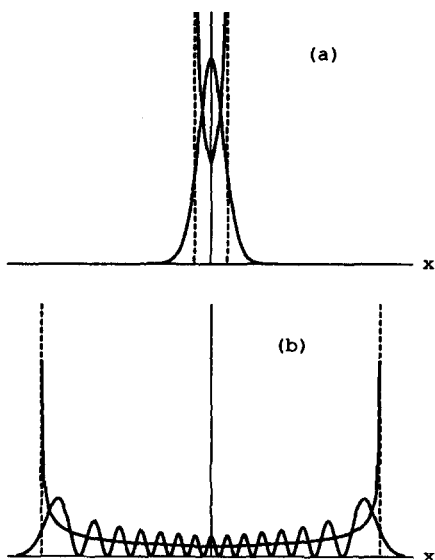


Fig. 7. The classical  $[P_{CL}(x)]$  and quantum  $[P_{QM}(x;n)=|\psi_n(x)|^2]$  position probability densities for the symmetric linear potential vs  $x$  for values of the quantum number  $n$  given by (a)  $n=0$  and (b)  $n=14$ .

$$P_{CL}(p) = \frac{1}{2p_0} \quad \text{for } |p| < p_0, \quad (53)$$

where  $A$  and  $p_0$  are the classical turning points for position and momentum, respectively, defined via  $E = F|A|$  and  $E = p_0^2/2m$ . The classical distributions are also plotted in Figs. 7 and 8 and once again show the appropriate correspondence principle behavior. The flat momentum dependence of  $P_{CL}(p)$  is consistent with the projection technique applied to Fig. 9(b) and is the analog of the constant  $x$  dependence of  $P_{CL}(x)$  for the infinite well. These classical distributions can

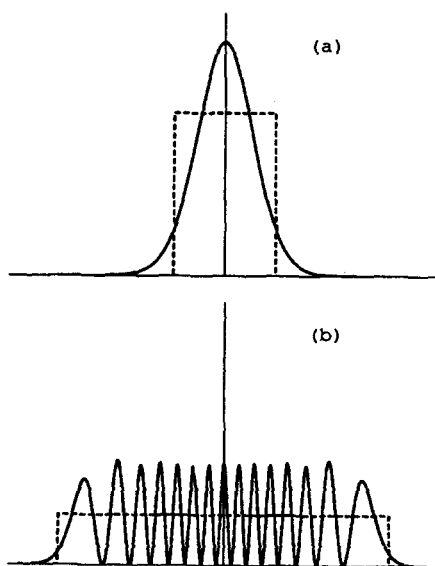


Fig. 8. The classical  $[P_{CL}(p)]$  and quantum  $[P_{QM}(p;n)=|\phi_n(p)|^2]$  momentum probability densities for the symmetric linear potential vs  $p$  for values of the quantum number  $n$  given by (a)  $n=0$  and (b)  $n=14$ . Note the flat momentum distribution emerging for large  $n$ .

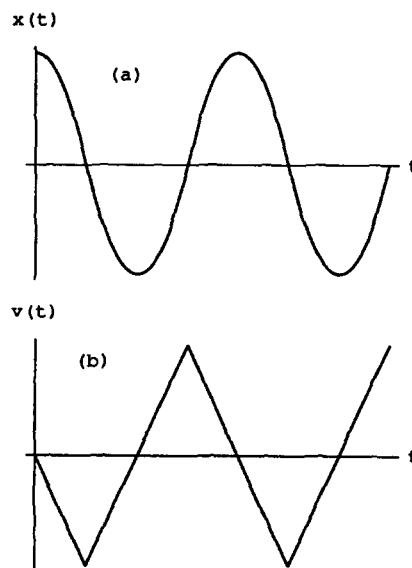


Fig. 9. The classical position  $x(t)$ , (a), and velocity  $v(t)$ , (b), for a particle in the symmetric linear potential. Note that the constant acceleration motion implies a straight line plot of the velocity which yields the constant momentum probability density using the projection technique.

be shown to imply that the energy is not shared equally as

$$\langle V \rangle = 2\langle T \rangle = \frac{2}{3}E, \quad (54)$$

which is consistent with virial theorem calculations.

We close by noting that power law potentials of the form  $V(x) = C|x|^\alpha$  can often be handled in a rather general fashion (by using, say, WKB techniques or, in three-dimensions, other semiclassical techniques.) For example, one can obtain simple scaling relations which give how the quantized energies scale with quantum number  $n$  (at least for  $n$  large!) or the mass  $m$ . For example, one can obtain

$$E_n \propto n^{2\alpha/(\alpha+2)} m^{-\alpha/(\alpha+2)}, \quad (55)$$

which reproduce the more exact results as can be checked for the cases of the harmonic oscillator ( $\alpha=2$ ), the linear potential ( $\alpha=1$ ), and the infinite well (using the limit  $\alpha \rightarrow +\infty$ ); they are even consistent with results (in 3D) for the Coulomb potential ( $\alpha=-1$ ). One can try to extend the analyses of classical distributions for position and momentum discussed here to the general value of  $\alpha$  and it is an instructive exercise to see how the  $\delta$ -function dependence of Eq. (40) is reached when  $\alpha \rightarrow \infty$ .

## V. THE "UNSTABLE" PARTICLE

One of the unique features of the harmonic oscillator is that it is exactly soluble at every level of mathematical sophistication from the simplest dimensional analysis arguments, to classical mechanics (in any formulation), quantum mechanics, and even in quantum field theory. Its physical relevance, however, comes from the fact that it represents the "best first guess" for the form of a potential near a point of stable equilibrium. The important distinction between stable and unstable equilibrium is a recurring theme in classical mechanics and in this section we extend the discussion of Sec. II to the case of the "unstable oscillator," i.e., a particle discussed by a harmonic oscillator potential of the "wrong

sign,” namely,  $V(x) = -kx^2/2$ . This also shows that such techniques can be applied even in the case of unbound motion.

The classical equation of motion in this case is

$$m\ddot{x}(t) = +kx(t) \quad (56)$$

which has the generic solution

$$x(t) = Ae^{-\omega t} + Be^{\omega t} \text{ or } x(t) = E \cosh(\omega t) + \sinh(\omega t). \quad (57)$$

Except for certain special cases, the general solution has the position coordinate increasing exponentially with time without bound.

For the quantum mechanical case, the dimensionless Schrödinger equation becomes

$$\frac{d^2\psi(y)}{dy^2} + y^2\psi(y) = -\epsilon\psi(y), \quad (58)$$

where  $\epsilon = 2E/\hbar\omega$ . Closed form solutions of this equation are possible and we only note here that the “oscillating” Gaussian wave packets (with macroscopic energy) derived in Ref. 2 can be trivially generalized to this case by letting  $k \rightarrow -k$  or  $\omega \rightarrow i\omega$  and exhibit exponential “runaway” behavior. Specifically, for the harmonic oscillator, solutions giving rise to the probability density

$$|\psi(x,t)|^2 = \frac{1}{L(t)\sqrt{\pi}} \exp\{-[x - (p_0/m\omega)\sin(\omega t)]^2/L^2(t)\}, \quad (59)$$

where  $L(t) = \sqrt{L^2 \cos^2(\omega t) + (\hbar/m\omega L)^2 \sin^2(\omega t)}$  can be taken over to the unstable oscillator case giving

$$|\psi(x,t)|^2 = \frac{1}{\tilde{L}(t)\sqrt{\pi}} \exp\{-[x - (p_0/m\omega)\sinh(\omega t)]^2/\tilde{L}^2(t)\} \quad (60)$$

with  $\tilde{L}(t) = \sqrt{L^2 \cosh^2(\omega t) + (\hbar/m\omega L)^2 \sinh^2(\omega t)}$ .

For purposes of visualization, we will not solve Eq. (58) completely but rather focus on the general properties of the solutions, especially for large  $|x|$ . A standard method of deriving the solution of the corresponding harmonic oscillator problem [i.e., Eq. (58) with the potential term changed in sign] is to begin by showing that the behavior of  $\psi(y)$  for large  $|y|$  is simply  $\exp(\pm y^2/2)$ ; the solution with the + sign must then be discarded as it diverges. Similarly, for Eq. (58) we find that for large  $|y|$

$$\psi(y) \rightarrow e^{\pm iy^2/2} \text{ or } \psi(y) \rightarrow \sin(y^2/2), \cos(y^2/2), \quad (61)$$

i.e., oscillatory solutions consistent with an unbound particle. For simplicity, we will specialize even further to the case of  $\epsilon \approx 0$ , corresponding to a classical particle “balancing” at the point of unstable equilibrium. In this case, we can get more information by assuming a solution of the form

$$\psi(y) = y^\alpha \sin(y^2/2) \quad (62)$$

and noting that

$$\begin{aligned} \psi''(y) + y^2\psi(y) &= (2\alpha + 1)y^\alpha \cos(y^2/2) \\ &\quad + \alpha(\alpha - 1)y^{\alpha-2} \sin(y^2/2) \\ &\approx 0 \text{ to } O(y^{\alpha-2}) \end{aligned} \quad (63)$$

provided  $\alpha = -1/2$ . Thus, the next better approximation gives

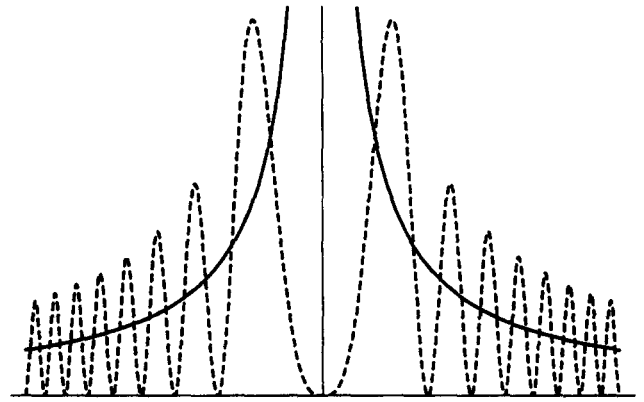


Fig. 10. The classical (solid curve) and quantum (dashed curve) representing the position-space probability density for the unstable or exponentially accelerating particle.

$$\psi(y) \propto \frac{\sin(y^2/2)}{\sqrt{y}} \left( \text{or } \frac{\cos(y^2/2)}{\sqrt{y}} \right), \quad (64)$$

which implies a probability density

$$P_{QM}(y) \propto \frac{\sin^2(y^2/2)}{y}. \quad (65)$$

This probability distribution is, of course, not normalized but can still be used to make connection with the classical motion of the particle.

To compare with the classical probability density, we note that for large time, any unstable solution will be dominated by the increasing exponential term, giving  $x(t) \rightarrow Be^{\omega t}$  so that

$$v(t) = \dot{x}(t) \rightarrow B\omega e^{\omega t} \propto x(t) \quad (66)$$

so that

$$P_{CL}(x) \propto \frac{1}{v(x)} \propto \frac{1}{x}. \quad (67)$$

Changing this to dimensionless variables and noting that the  $\sin^2(y^2/2)$  term averages to 1/2 over many cycles, we can compare the quantum and classical probability distributions for an unstable particle, namely

$$P_{CL}(y) \propto \frac{1}{2y} \text{ and } P_{QM}(y) \propto \frac{\sin^2(y^2/2)}{y}, \quad (68)$$

which we plot in Fig. 10. Once again, the increasing wiggleness as  $|y|$  (and hence  $|x|$ ) increases is indicative of increasing kinetic energy while the decreasing amplitude is consistent with less and less time spent in a given  $y$  interval, i.e., larger speeds. This, then, is the quantum mechanical “picture” of particle “rolling off a log.” We note that this special case of  $E = 0$  is not strictly in what is usually thought of as the correspondence principle regime of “ $E$  large.” As the particle accelerates away from the origin, however, the magnitude of both its kinetic and potential energies increase at an exponential rate, becoming arbitrarily large. This is one reason why we focus on the large  $|x|$  limit for the quantum-classical comparison; in this case, the origin is almost a classical turning point where we would expect the analogy to fail. The interested reader can also examine the quantum and



classical probability densities for potential and kinetic energy in this case.

Finally, we note that the symmetry between  $x$  and  $p$  in the differential equation implies that the classical momentum distribution will also be of the form

$$P_{QM}(q) \propto \frac{\sin^2(q^2/2)}{q}, \quad (69)$$

where  $q$  is the scaled momentum of Eq. (24). The classical momentum distribution requires

$$P_{CL}(p) \propto \frac{1}{F(x)} \propto \frac{1}{a(t)} \propto \frac{1}{p(t)} \propto \frac{1}{p} \quad (70)$$

using  $F=ma$  and the fact that the acceleration,  $a(t)$ , as well as  $x(t)$  and  $v(t)=p(t)/m$  are all exponentially increasing functions in time. Thus

$$P_{CL}(q) \propto \frac{1}{2q}, \quad P_{QM}(q) \propto \frac{\sin^2(q^2/2)}{q} \quad (71)$$

and we obtain the same behavior as seen in Fig. 10.

## VI. THE UNIFORMLY ACCELERATING PARTICLE

The case of constant acceleration in one dimension is a standard topic in any introductory course in classical mechanics and we consider the corresponding classical and quantum probability distributions as our final example. To be consistent with the notation and results of Sec. IV, we choose the potential to be  $V(x)=Fx$  with  $F>0$  which implies a constant force given by  $F(x)=-F$ , i.e., uniform acceleration to the left.

The corresponding Schrödinger equation is just Eq. (45), namely

$$\frac{d^2 \psi(y)}{dy^2} = y \psi(y) \quad (72)$$

but now defined for all values of  $y$ . The solutions are the  $Ai(y)$  and  $Bi(y)$  shown in Fig. 6 and we will briefly derive some of the properties of these functions, especially for large  $y$ . For  $y>0$ , by analogy with the standard differential equation,  $f''(x)=+k^2 f(x)$  which has the exponential solutions  $f(x)=\exp(\pm kx)$ , we might expect a similar exponential dependence and it is easy to show that the large  $y$  form of the solutions to Eq. (72) is simply

$$\psi(y) \rightarrow e^{\pm 2y^{3/2}/3} \quad \text{for } y \gg 0. \quad (73)$$

The  $Bi(y)$  solution corresponds to the exponentially growing solution and must be discarded in this case while the  $Ai(y)$  evidences exponential tunneling into the  $V(x)=Fx$  potential barrier. For large negative  $y$ , one finds the oscillatory solutions

$$\psi(y) \rightarrow e^{\pm i 2y^{3/2}/3} \quad \text{or} \quad \sin\left(\frac{2y^{3/2}}{3}\right), \cos\left(\frac{2y^{3/2}}{3}\right) \quad (74)$$

for  $y \ll 0$ . Following the method of the last section, we can obtain a more complete result by assuming a form

$$\psi(y) = y^\alpha e^{i 2y^{3/2}/3} \quad (75)$$

and find that  $\alpha=-1/4$ . These results are consistent with the "handbook limits,"<sup>17</sup> namely

$$Ai(z) \rightarrow \frac{1}{2} \frac{1}{\sqrt{\pi \sqrt{z}}} e^{-\zeta} \left[ 1 - \frac{c_1}{\zeta} + \dots \right], \quad (76)$$

$$Ai(-z) \rightarrow \frac{1}{\sqrt{\pi \sqrt{z}}} \left[ \sin\left(\zeta + \frac{\pi}{4}\right) - \cos\left(\zeta + \frac{\pi}{4}\right) \frac{c_1}{\zeta} + \dots \right], \quad (77)$$

where  $\zeta=2z^{3/2}/3$  and  $c_1=5/72$  and with Fig. 6.

While these stationary state solutions cannot be normalized, we can make use of these results to show that the quantum probability density is given by

$$P_{QM}(y) \propto \frac{\sin^2(2y^{3/2}/3 + \pi/4)}{\sqrt{y}} + \dots \rightarrow \frac{1}{2\sqrt{y}}, \quad (78)$$

when one averages over several cycles. This can then be easily compared to the classical result since  $x(t)=at^2/2$  and  $v(t)=at$  (assuming no initial velocity) so that  $v(x) \propto \sqrt{x}$  and

$$P_{CL}(x) \propto \frac{1}{v(x)} \propto \frac{1}{\sqrt{x}}, \quad (79)$$

which has the same form as Eq. (78). The usual arguments about the wiggleness and magnitude of  $\psi(x)$  expressing the increasing speed of the particle as it accelerates toward the left can now be easily visualized in Fig. 6. The seemingly dramatic difference between the motions of the exponentially accelerating particle versus one with constant acceleration, i.e.,  $x(t) \propto e^{\omega t}$  in contrast to  $x(t) \propto t^2$ , appears as a rather subtle difference in quantum wave functions,  $\psi(x) \propto 1/\sqrt{x}$  vs  $1/\sqrt[4]{x}$ .

Finally, the Schrödinger equation in momentum space corresponding to uniform acceleration, namely

$$\frac{p^2}{2m} \phi(p) - iF\hbar \frac{d\phi(p)}{dp} = E \phi(p) \quad (80)$$

has solutions which are simple phases,

$$\phi(p) \propto e^{i(p^3/6m - Ep)/\hbar F}, \quad (81)$$

which implies that the quantum momentum probability density,  $|\phi(p)|^2$  (once again, not normalizable) is constant. This is, of course, consistent with the classical result

$$P_{CL}(p) \propto \frac{1}{F(x)} = \frac{1}{F} \propto \text{const.} \quad (82)$$

The Airy functions play several interesting roles in quantum mechanics besides describing the position-space wave function of an accelerating particle. They are necessarily used in comprehensive discussions of the WKB method<sup>18</sup> where the formulas connecting wave functions inside and outside a well are derived and they also appear in more subtle discussions of the weak equivalence principle<sup>19</sup> in quantum mechanics. It can be interesting to the student to see that the mathematical form (magnitude and wiggleness) of the Airy solutions has a physical meaning consistent with one of the most familiar of all mechanical systems.

<sup>1</sup>See, e.g., R. Liboff, *Introductory Quantum Mechanics* (Addison-Wesley, Reading, MA, 1980), pp. 151–155.

<sup>2</sup>D. S. Saxon, *Elementary Quantum Mechanics* (McGraw-Hill, New York, 1968), pp. 144–147.

<sup>3</sup>S. Howard and S. K. Roy, "Coherent states of a harmonic oscillator," *Am. J. Phys.* **55**, 1109–1117 (1987).

<sup>4</sup>P. J. E. Peebles, *Quantum Mechanics* (Princeton University Press, Princeton, 1992), pp. 167–170.

- <sup>5</sup>A. Goldberg, H. M. Schey, and J. L. Schwartz, "Computer-generated motion pictures of one-dimensional quantum-mechanical transmission and reflection phenomena," *Am. J. Phys.* **35**, 177–186 (1967); "One-dimensional scattering in configuration space and momentum space," *ibid.* **36**, 454–455 (1968).
- <sup>6</sup>M. H. Bramball and B. M. Casper, "Reflections on a wave packet approach to quantum mechanical barrier penetration," *Am. J. Phys.* **38**, 1136–1145 (1970).
- <sup>7</sup>J. R. Merrill, "The propagation of quantum mechanical wave packets," *Am. J. Phys.* **41**, 1101–1103 (1973).
- <sup>8</sup>J. S. Boleman and S. B. Haley, "More time-dependent calculations for the Schrödinger equation," *Am. J. Phys.* **43**, 270–271 (1975).
- <sup>9</sup>C. Segre and J. D. Sullivan, "Bound-state wave packets," *Am. J. Phys.* **44**, 729–732 (1976).
- <sup>10</sup>E. A. Johnson and H. T. Williams, "Quantum solutions for a symmetric double square well," *Am. J. Phys.* **50**, 239–243 (1982).
- <sup>11</sup>I. Galbraith, Y. S. Ching, and E. Abraham, "Two-dimensional time-dependent quantum-mechanical scattering event," *Am. J. Phys.* **52**, 60–68 (1983).
- <sup>12</sup>See, e.g., Ref. 1, pp. 192–195.
- <sup>13</sup>The momentum-space wave functions for scattering are briefly discussed and illustrated in the second reference of Ref. 5.
- <sup>14</sup>A. Goswami, *Quantum Mechanics* (Brown, Dubuque, 1992), pp. 88–91.
- <sup>15</sup>R. Winter, *Quantum Physics* (Wadsworth, Belmont, 1979), pp. 92–97.
- <sup>16</sup>S. Wolfram, *Mathematica: A System for Doing Mathematics by Computer* (Addison-Wesley, Reading, MA, 1991).
- <sup>17</sup>M. Abramowitz and I. A. Stegun, *Handbook of Mathematical Functions* (National Bureau of Standards, Washington, D.C., 1964), pp. 446–449.
- <sup>18</sup>D. Park, *Introduction to the Quantum Theory* (McGraw-Hill, New York, 1992), 3rd ed., pp. 106–109.
- <sup>19</sup>B. Holstein, *Topics in Advanced Quantum Mechanics* (Addison-Wesley, Reading, MA, 1992), pp. 108–110.

## Control of the chaotic driven pendulum

Gregory L. Baker

*College of the Academy of the New Church, Bryn Athyn, Pennsylvania 19009*

(Received 23 March 1994; accepted 21 December 1994)

A method of controlling chaos (due to Ott, Grebogi, and Yorke) is illustrated with a simulated chaotic pendulum. The method consists of stabilizing a previously unstable periodic orbit through a feedback mechanism that periodically adjusts the damping parameter of the pendulum. The presentation is pedagogical and describes the method in more detail than is typical of the research literature on controlling chaotic systems. © 1995 American Association of Physics Teachers.

### I. INTRODUCTION

The pendulum has long served as a pedagogically useful model in mechanics. From Galileo's discovery of the approximate constancy of its period for small oscillations,<sup>1</sup> to its recent use as an experimental<sup>2</sup> and simulation model<sup>3,4</sup> for nonlinear dynamics, the pendulum has exhibited a rich variety of dynamical behavior. The pendulum has for many decades exemplified periodic motion,<sup>5</sup> and its more recent emergence as a primary example of chaotic dynamics has made it ubiquitous in the mushrooming pedagogical literature on chaotic dynamics.<sup>3,6,7</sup> In this paper we use the pendulum to illustrate the "control of chaos."

The control of physical systems is an important subject in engineering, and the classical literature is extensive.<sup>8</sup> However the application of control algorithms to chaotic dynamics is recent. The goal is to continually but slightly perturb a chaotic mechanical system so as to cause it to act nonchaotically. More precisely, the parameters of the system are such that it would ordinarily exhibit chaos and yet the system can be made to behave periodically by a time-varying adjustment of the parameters *in the chaotic range*. The requisite size of the perturbation depends on the momentary deviation from periodicity, and therefore the control mechanism is a version of proportional feedback.

This and other similar control algorithms may have important application in a variety of areas where chaotic signals are present.<sup>9</sup> Typical examples include possible control of cardiac fibrillation, epileptic seizures, and chemical reactions.<sup>10</sup> Control may also be used to extend the stability

regime of lasers<sup>11</sup> and has even been suggested as a strategy for efficient vaccination of populations against various diseases.<sup>12</sup>

While several control mechanisms for chaotic systems are known, we confine our discussion to the elegant scheme proposed by Ott, Grebogi, and Yorke<sup>13</sup> (OGY) in 1990 and very quickly applied to a physical system, the magnetoelastic ribbon, by Ditto, Rauseo, and Spano.<sup>9,14</sup> Variations of the OGY scheme have been applied to other oscillating systems. For example, control of a "parametric" pendulum—one whose pivot point is driven vertically—has been achieved both in experiment and numerical simulation by Starrett and Tagg.<sup>15</sup> Nitsche and Dressler have achieved control when the dynamical system is known only by a time series. They applied their modification of OGY control to a time series from a simulated Duffing oscillator.<sup>16</sup> Finally, Hubinger, Doerner, and Martienssen<sup>17</sup> used an extension of the OGY method (involving quasicontinuous control) to control an experimental pendulum.

In the original paper the OGY method was applied to the two-dimensional Henon map. Here we take a similar approach and use the Poincaré section of the forced, damped pendulum as a two-dimensional map.

We begin with a brief description of the simulated driven pendulum. Then two representations of chaotic behavior are described: (1) a *bifurcation diagram* which displays dynamical behavior over a range of control parameter values, and (2) a *Poincaré section* which shows periodic sampling of the state variables, angle  $\theta_n$ , and angular velocity  $\omega_n$ . Finally, the OGY algorithm is applied to the pendulum—in part, to